Composites Science and Technology 90 (2014) 154–159

Contents lists available at ScienceDirect

Composites Science and Technology

journal homepage: www.elsevier.com/locate/compscitech

Novel, highly-filled ceramic–polymer composites synthesized by a spouted bed spray granulation process

M.F.H. Wolff [a], V. Salikov [a], S. Antonyuk [a], S. Heinrich [a,*], G.A. Schneider [b]

[a] Hamburg University of Technology, Institute of Solids Process Engineering and Particle Technology, Denickestr. 15, 21073 Hamburg, Germany
[b] Hamburg University of Technology, Institute of Advanced Ceramics, Denickestr. 15, 21073 Hamburg, Germany

ARTICLE INFO

Article history:
Received 26 March 2013
Received in revised form 4 November 2013
Accepted 9 November 2013
Available online 20 November 2013

Keywords:
Spouted bed
Granulation
Composite
Filling degree
B. Mechanical properties

ABSTRACT

We present a novel processing route to synthesize homogeneous ceramic polymer composites with ultra-high (~78 vol.%) packing density by using the spouted bed granulation technology and subsequent warm pressing. In the granulation process, two ceramic particle size fractions (α-Al_2O_3) and a thermoplastic polymer (polyvinyl butyral) are assembled to granules. In the process, μm-sized particles are coated with a layer of polymer which contains a second, nm-sized ceramic particles fraction. The mass fractions of each constituents can be adjusted independently. During the warm pressing, the nm-sized particle fraction along with polymer is pressed into the void volume of the μm-sized particles, thus achieving a homogeneous, isotropic composite structure with a very high packing density of ceramic particles. The material, which can easily be produced in large quantities, combines a high modulus of elasticity (up to 69 GPa), tensile strength (~50 MPa), and pronounced fracture strain (~0.1%) with an isotropic, biocompatible, metal-free composition. Possible failure mechanisms are discussed, including failure due to necking of the polymer, and failure due to limited polymer–particle-interfacial strength.

1. Introduction

Ceramic materials are intensively studied and used for applications in materials sciences and industries. The versatile use of this material class is a consequence of a number of useful properties such as high hardness and modulus of elasticity, and its abundance in nature. However, the structural applications of ceramic materials are often limited by their high brittleness and scatter of mechanical properties resulting in the lack of predictability of the material failure. On the other hand, polymeric materials in general exhibit a number of properties which are more or less complementary to the ones of ceramic materials, such as high ductility, adjustability, but relatively low modulus of elasticity and strength. These two materials classes are therefore often combined to form composite materials, and also both occur in many biological materials, in which large amounts of minerals are combined with small amounts of proteins or biopolymers. One of the most astounding findings in materials such as nacre has been, apart from discovering their hierarchical structure, the very high volume fraction of stiff constituents in a polymeric matrix, which is far beyond current technological capacities of materials design. Nacre for example consists of about 95 vol.% calcium carbonate and about 5 vol.% of polymeric material [1,2]. In general, the outstanding mechanical properties of these materials seem to be a complex interplay between their composite morphology, interface properties, and hierarchical assembly [3–8]. Inspired by nature's design principle, there has been much progress in synthesizing ceramic polymer composite materials [9–15], and exceedingly high values for toughness [16], dielectric constant [17], and strength [18] have been reported. However, the reported volume fractions for particles [13], platelets [19], and fibers [20] as reinforcing phase are always very much lower than in biological materials, resulting e.g. in a deficiency of the stiffness at least in one dimension. The stiffness of the polymeric phase can be slightly enhanced by cross-linking [18], but such techniques are tedious for bulk samples and have the tendency to be non-biocompatible. The way to achieve very high (isotropic) stiffness is therefore to achieve a very high packing density of the stiff phase in a composite. The isotropy is an inherent property of the composite when the filler material has a particulate nature (unlike e.g. fibers) and the filler material is homogeneously distributed within the polymer. It is known that in order to reach packing densities > 70 vol.% using nearly spherical particles, at least two particles size fractions have to be combined such that the void volume of one fraction is filled by the other (smaller) one [21,22]. This has proven to be very difficult to accomplish homogeneously for macroscopic amounts of material. Most of the experimental techniques and theoretical

* Corresponding author. Tel.: +49 40428783750.
E-mail address: stefan.heinrich@tuhh.de (S. Heinrich).

0266-3538
http://dx.doi.org/10.1016/j.compscitech.2013.11.006

investigations in the literature have therefore focused on small and medium filling degrees. At the same time the amount of polymer should be adjusted to exactly fill the free gap volume. This is vital for enhancing the fracture strain and avoiding large pores which would lower the strength of the material. While in the literature large enhancement factors for the stiffness are reported in composites, they are typically limited to one dimension (e.g. when fibers are used). However for particulate (low-aspect ratio-) filler particles, the composite material basically has the same modulus of elasticity in all spacial directions, which means that also two- and three-dimensional states of stress can be sustained, which is a considerable advantage for the design of structural elements, which often undergo complex states of stress. Another advantage of particulate filler particles as opposed to fibers is the generally much better biocompatibility, which opens up applications such as tooth implants, and which also simplifies the disposal of the material, a factor of ongoing increasing importance.

We developed a novel processing route combining the spouted bed technology [23,24] and subsequent warm pressing, with which it is possible to synthesize a microstructured ceramic–polymer composite material with very high filling degree and very small porosity, which is far more than reliably reported so far in the literature. In the granulation process, two ceramic particle size fractions (α-Al_2O_3) and a thermoplastic polymer (polyvinyl butyral) are assembled and then compressed to form a dense composite material. The material, which can easily be produced in macroscopic amounts, combines a high elastic modulus, tensile strength, and pronounced fracture strain with an isotropic, biocompatible, metal-free composition. As each of the components can be adjusted individually during the granulation process, the granules can be designed to have optimized properties (composition and morphology) for the subsequent uniaxial warm pressing. Spouted beds are in general known for their good mixing of the solid phase and are often used for the granulation and agglomeration of food powders, fine chemicals and pharmaceutical powders [25–29], but have not been used so far for the synthesis of microstructured composite materials. The technique consists of three basic steps: (1) preparation of the polymer solution, (2) spouted bed spray granulation, and (3) warm pressing. These processes as well as the structural and mechanical characterization methods are described in Section 2. In Section 3, the results of the granulation process and of the mechanical characterization are analyzed, and possible material failure mechanisms are discussed, including failure due to the propagation of cracks, and failure due to necking of the polymer.

2. Materials and methods

2.1. Materials

All ceramic particle fractions consisted of α-Al_2O_3, which has a modulus of elasticity of between 350 and 400 GPa, a density of about 3.98 g/cm^3, and no measurable fracture strain. The fluidized particles were fused alumina F360 (Kuhmichel Abrasiv GmbH) with a nominal $d_{50,3}$ of (22.8 ± 1.5) μm. The particle size distribution of these particles was measured with a camsizer XT (Retsch Technology GmbH). The particles used for the suspension were CT 3000 SG from Almatis Inc. ($d_{50,3} \sim 500$ nm), except for the lowest-filled samples, for which Alumina microgrid WCA 5 ($d_{50,3} \sim 4$ μm) from Pieplow & Brandt GmbH, Germany, was used. The used polymer was polyvinyl butyral (PVB) Mowital B 30 H, which was provided by Kuraray Europe GmbH. This polymer type has a medium degree of acetalization, a glass transition temperature of 68 °C, and, according to the manufacturer, a modulus of elasticity of approx. 2.5 GPa, a yield stress of 58 MPa, a tensile strength of 34.8 MPa, and an elongation at break of 57.9%. Ethanol was used as solvent, and diluted hydrochloric acid was used to adjust the pH value of the polymer–particle suspension. The ceramic Al_2O_3 is a versatile and frequently used technical ceramic, as it offers high hardness, strength, and modulus of elasticity, it is non-hazardous to health. The polymer (PVB) was chosen because it offers a good combination of properties, in particular it has a very good adhesion to hydrophilic surfaces and good solving properties.

2.2. Preparation of the polymer solution

To prepare the polymer solution, between 28 g and 42 g of the PVB were dissolved in ethanol with concentrations of 4–6 wt.%. 145 g of α-Al_2O_3 particles of the finer fraction were then added to the solution, and a heated ultrasonic bath was used for deagglomeration. For the stabilization of the suspension, diluted hydrochloric acid was added to reduce the pH value of the suspension from near the isoelectric point of alumina (pH ∼ 9) [30] to about pH 6. The suspension was then put on a heated magnetic stirrer and sprayed onto the fluidized alumina particles of the coarser fraction in the spouted bed apparatus using a peristaltic pump and a two-component nozzle.

2.3. Spouted bed spray granulation

300 g Of α-Al_2O_3 particles of the coarse fraction were fluidized in a prismatic spouted bed apparatus [31,32] (Fig. 1) with a small process chamber and a steep and large expansion zone (cross-section area ratio ∼13.8) described in [33], particularly constructed for the processing of fine and ultrafine particles (Geldart group C [34]) which cannot be fluidized in conventional fluidized beds [35]. The process gas (ambient air) was slightly heated to reach a temperature in the fluidizing zone of about 40 °C. The ceramic particles were fluidized in the dilute spouting regime (also called jet-spouting [36]) and were layered in the spray granulation process by the injected droplets containing the suspended ceramic particle fraction and the dissolved polymer, while the solvent evaporated and left the apparatus along with the process gas. Because of the small size and adhesion forces, a certain amount of agglomeration of the coated particles took place, which however did not significantly disturb the granulation process. Due to the intensive mixing as well as heat and mass transfer in the spouted bed spray granulation process, a homogeneous mixing of different particle sizes and the polymer was achieved, and segregation was avoided.

2.4. Uniaxial warm pressing

10–20 g Of the granules were then given into a steal die (inner diameter 4 cm) for warm pressing. At a pressure of 40 MPa the temperature was increased by ∼5 K/min to its final temperature of 160 °C. The pressure was then increased to 750 MPa. After 1 h, the sample was instantaneously unloaded and slowly cooled down to room temperature.

2.5. Compositional and mechanical analysis

The composition of the material was analyzed by measuring the geometrical density of the pressed sample and the non-volatile weight fraction. This was done by heating 5–10 g of the same granules to a temperature (600 °C) clearly above the decomposition temperature of the polymer (ash content of PVB < 0.1 wt.% at T = 600 °C) and measuring the relative weight loss. The ceramic volume fraction $p_{\mathrm{vol}}^{\mathrm{cer}}$ was then calculated via $p_{\mathrm{vol}}^{\mathrm{cer}} = w_{\mathrm{cer}} \cdot \rho_{\mathrm{press}}/\rho_{\mathrm{cer}}$, where $w_{\mathrm{cer}} = m_{600^\circ\mathrm{C}}/m_{\mathrm{room\ T}}$ is the residual mass fraction of the granules, $\rho_{\mathrm{press}} = m_{\mathrm{press}}/V_{\mathrm{press}}$ is the density of the pressed sample, and $\rho_{\mathrm{cer}} \simeq 3.98$ g/cm^3 the density of α-Al_2O_3. The polymeric volume fraction was calculated correspondingly by using

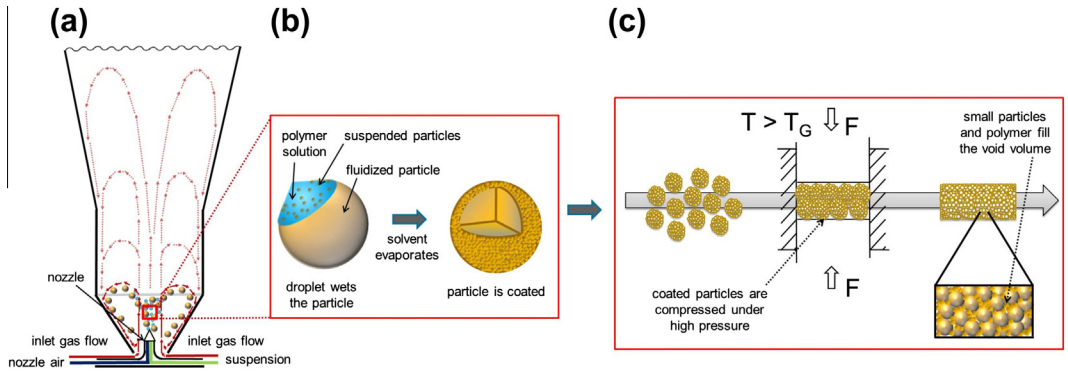

Fig. 1. Sketch of the spouted bed granulation process. (a) The coarser ceramic particle fraction is fluidized in the spouted bed apparatus. (b) The second, smaller ceramic particle fraction is suspended in a polymer solution and sprayed into the spouted bed, forming layers on the surface of the fluidized particles. (c) The layered granules are then compressed under high pressure at a temperature between the glass transition temperature and the decomposition temperature of the polymer.

$w_{pol} = 1 - w_{cer}$ and replacing ρ_{cer} by $\rho_{pol} \simeq 1.1$ g/cm^3 in the above equation. Thermogravimetric analysis (TGA) was several times additionally carried out before and after the compression yielding very similar results. The porosity ε was calculated via $\varepsilon = (V_{press} - V_{cer} - V_{pol})/V_{press}$. TGA was also used to verify the absence of appreciable amounts of volatile mass fractions in the ceramic particles as well as the negligible ash content of the polymer, as well as to determine the begin of the polymer decomposition, which set an upper limit for the temperature during the warm pressing.

For four-point bending, the pressed samples were grinded and cut into beams of approx. $2 \times 2 \times 30$ mm^{3}using a diamond saw, and tested with a custom-made four-point-bending device, which is described in detail in [37]. The modulus of elasticity was calculated according to Bernoulli–Euler beam theory [38] within the linear part of the obtained force–displacement curves:

$$E_{bending} = \frac{La^2 \Delta F^{tot}}{4I\Delta z}\left(1 - \frac{4a}{3L}\right) \quad (1)$$

where $\Delta F^{tot} = \Delta(F^{load\ 1} + F^{load\ 2})$ being the sum of the forces acting on each support, $a = 10$ mm is the distance between lower and upper support, L is the distance between the upper supports, and I is the second moment of area, with $I = 1/12wh^3$ for a beam of width w and height h. Tensile testing was done using a Zwick Roell zwickiLine Z2.5 testing machine at an effective strain rate of approx. 0.02–0.05%/min (constant nominal tensile speed). The samples were cut into rods of about 1.7×4.8 mm^2 cross section and were bonded onto metal holders, which were connected to a rope on one side to minimize other loads due to imperfect positioning of the sample. The strain was measured optically with a video extensometer by placing two optical markers onto the samples.

3. Results and discussion

3.1. Compositional analysis

Fig. 2 shows the structure of the granules after the granulation process and before the warm pressing. The polymer solution with the second, nm-sized particle fraction built a film around the larger fluidized particles, which also slightly agglomerated during the process.

The resulting very high filling degrees of 78 vol.% after the warm pressing as well as SEM analysis (Fig. 5) clearly indicate that the fine (0.2–0.5 μm) particle fraction coating the coarse (~23 μm) particle fraction was preferentially pressed into the void volume of this larger particle fraction, thus achieving a very high packing density and homogenous mixture of the hard and soft phases within the material. The volume content of the polymeric phase was chosen during the granulation process to exactly fill the remaining void volume (approx. 15–20 vol.%, as this is the typical void volume in a random dense packing of two different particle size fractions [21]). The very high, unprecedented value of the packing density which was achieved with μm- and nm-sized particles along with a finely dispersed polymer is a result of the intensive heat and mass transfer as well as mixing properties of the spouted bed spray granulation process. This can be better understood if one looks at an individual particle of the fluidized fraction: at the instance when the fluidized particle is combined with the small particle fraction and polymer by the droplet–particle-interaction in the spraying zone, the particle is not exposed to any external forces such as apparatus walls or particle–particle-contacts. As the solvent in the droplet then rapidly evaporates and the polymer immediately starts to act as a solid binder, the structure of the coated granule is maintained during subsequent collisions with other

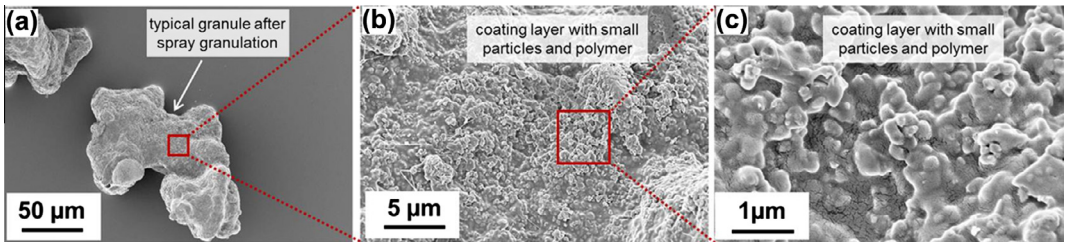

Fig. 2. (a) Scanning electron micrographs of granules after the spouted bed spray granulation process, and before the warm pressing. (b and c) Close-up view onto the surface of the granules shows the dried polymer–embedded ceramic particle fraction.

Table 1
Mechanical properties of the produced composites.

Ceramic fraction ρ_{cer} (vol.%)	Porosity ε (vol.%)	Bending modulus E_{bend} (GPa)	Tensile modulus E_{tens} (GPa)	Fracture strain ε_{fr} (%)
65.7	3.5		30 ± 6	0.15
69.3	3	33 ± 4	36 ± 4	0.12
70.9	2.1	41 ± 3		
76.3	4.7	49 ± 3	69 ± 10	0.06
77.6	1.4	63 ± 2		

particles or apparatus walls. Table 1 lists the obtained data from compositional and mechanical analysis for typical samples. The statistical errors are given as standard deviation. For comparison, the granulation process was also carried out without adding the second particle size fraction into the dissolved polymer, and packing densities of pressed samples of max. 71 vol.% were achieved. In order to obtain larger sample sizes, the diameter of the press matrix can be increased (higher sample diameter), and a higher amount of granules can be used (larger sample height), but higher force (higher pressure) might be necessary to reach the same filling degree. The amounts of materials were chosen in such a way that the desired filling degree was reached. To ensure that enough polymer is available in the sample, the amount of polymer which was sprayed onto the coarse particle fraction was chosen to be higher than the theoretical total void volume. For the samples with the highest filling degrees, 28 g of PVB were used for the fixed 300 g of fluidized coarse particles. Smaller filling degrees were reached by spraying more polymer onto the particles (42 g for the samples with medium filling degree around 70 vol.%). The excess amount of polymer is in accordance with a smaller filling degree, as it prevented the ceramic particles from a closer packing. The smallest filling degrees were reached by additionally choosing a larger particle size for the finer particle fraction ($d_{50,3} \sim 4$ µm instead of $d_{50,3} \sim 500$ nm), as a smaller particle size ratio between the two fractions leads to a smaller filling degree [21]. The amount of coarse particles (300 g) was chosen to enable good fluidization properties in the spouted bed apparatus, and the ratio of coarse to fine particle was chosen to be in the range between 60% and 70%, as this is the optimum ratio for the packing of two particle size fractions [21]. The measured value for the medium particle size ($d_{50,3} = 26$ µm) was slightly larger than the literature value (22.8 ± 1.5 µm), possibly due to imperfect separation during measurement. The distribution of particle sizes was measured to be moderately large, with a $d_{10,3} = 17$ µm and a $d_{90,3} = 37$ µm. As a spread in particle size aids the packing of one particulate phase [21], this is in accordance with the fact that higher packing densities than 64 vol.% were achieved without a second ceramic phase.

Fig. 3 shows the typical behavior in thermogravimetric analysis of the ceramic particles, the polymer, and coated granules after the granulation process. As can be seen, the polymer starts to decompose at a temperature around 200 °C, and then degrades in a two-step process, until at about 550 °C only a negligible ash content is left over. Incidentally, the slow-down of the degradation at about 20 wt.% is in good agreement with the amount of hydrophilic polyvinyl alcohol groups in the PVB, which is between 18 and 21 wt.% for this particular type. The pressing temperature was chosen to be 160 °C, as this is well above the glass transition temperature of the polymer, but clearly lower than the temperature at which the polymer starts to decompose.

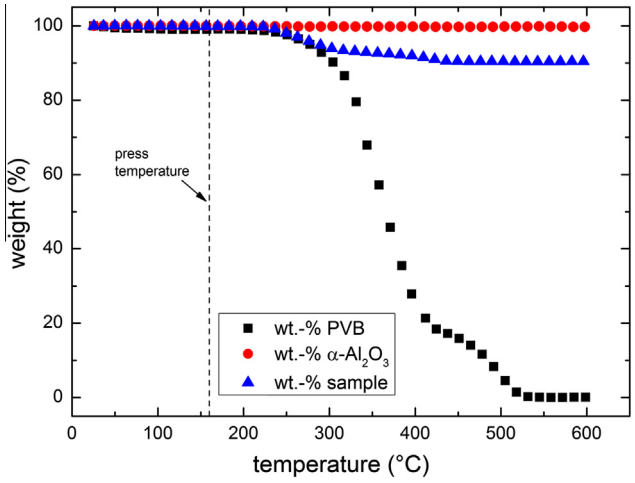

Fig. 3. Thermogravimetric analysis of the polymer (black squares), the α-Al_2O_3 (red dots), and composite granules which contain about 90 wt.% of ceramic particles (blue triangles). (For interpretation of the references to colour in this figure legend, the reader is referred to the web version of this article.)

3.2. Mechanical testing

Fig. 4 shows the measured modulus of elasticity in four-point-bending and tensile testing (a) and the stress–strain curves obtained by tensile testing (b) for samples of different filling degree. As expected from the rule of mixtures, the bending and tensile moduli increase monotonically with increasing ceramic amount and reach values of 63 and 69 GPa for filling degrees of ~76 to 78 vol.% (Fig. 4a). While the bending tests were suitable for determining the modulus of elasticity, they did however not accurately yield the strength and fracture strain of the samples, because the inelastic deformations implied that the loading scheme for large displacements was a combination of bending stress and tensile stress, for which the bending theory is no longer reliably applicable. These were therefore measured in tensile testing. The stress–strain curves in Fig. 4b illustrate the polymer-induced transition from linear-elastic to plastic deformation for high loads before failure, which is very desirable for materials design, but is not accomplished in purely ceramic materials. The stress–strain curves measured in tensile testing show that the strength of the material is narrowly distributed and essentially controlled by the polymer (polymer yield strength 58 MPa, tensile breaking stress 34.8 MPa). Very similar inelastic behavior for high loads was also observed in 4-point bending measurements, and the force–displacement curves yielded bending strengths between 103 and 129 Mpa when calculated according to Bernoulli–Euler beam theory. For the highest packing densities, the modulus of elasticity is increased by a factor of more than 25 compared to the polymer, which, due to the symmetrical particulate nature of the filler particles and their homogeneous distribution within the material, should be the same or at least very similar for any direction of loading.

3.3. Failure mechanism

Unlike in ceramics, the mechanical failure of polymers is typically induced by the sliding of polymer chains relative to each other. This leads to a smaller strength compared to ceramics, but also to much larger inelastic deformation prior to failure. As is

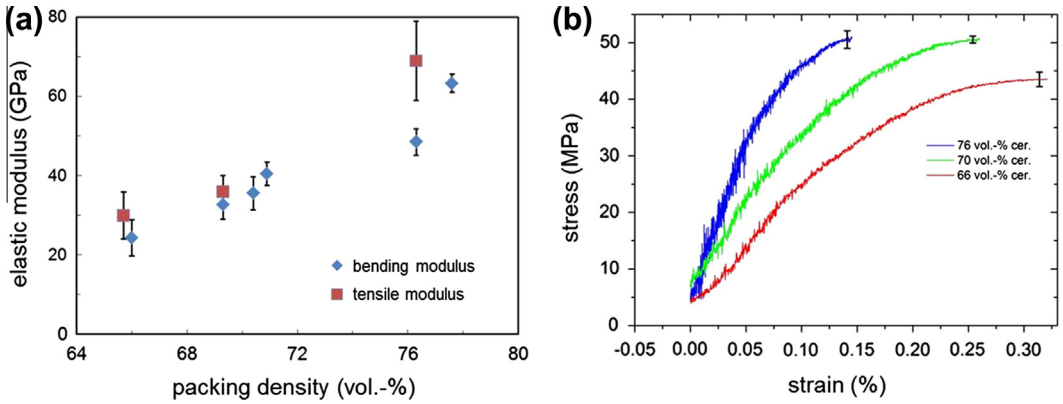

Fig. 4. (a) Modulus of elasticity E versus packing density measured in four-point bending (rhombuses) and tensile (squares) testing. (b) Stress–strain curves from tensile testing for 3 different packing densities (66, 70, and 76 vol.% ceramic).

known from the literature, almost all of the inelastic deformation is lost when samples are filled with substantial volume fractions of filler materials. Wang et al. [39] for example measured a reduction of fracture strain from >300% to below 2% (factor > 150) for a filling degree of 45 vol.%. For platelets, Bonderer et al. [19] measured a fracture strain of <5% for a filling degree of 0.4, while the unfilled polymer matrix had a fracture strain of >1000%, which corresponds to a reduction of fracture strain by a factor of >200. The thermoplast PVB which was used in this study has in general a fairly large elongation at break of >50%. The exact value depends on the polymer specification and is about 57.9% for the used polymer type. The relatively small fracture strain of <0.2% which was measured is thus in accordance with the generally observed phenomenon of large reductions of fracture strain in highly-filled composites, and clearly points out that most of the polymer is not loaded to its yield point. There are basically three possible mechanisms which can lead to such a behavior: (1) brittle failure due to unstable crack propagation, (2) detachment at the particle–polymer interface, and (3) strongly reduced plastic deformation of the polymer due to the presence of nanoparticles. In the following all three mechanisms are discussed. (1) Due to the high amount of ceramics, brittle failure may occur by crack propagation through the polymer. As is known from fracture mechanics [40], the crack length $2a$ for which a material with given strength σ_c and toughness K_{Ic} fails due to crack propagation is given for a Griffith crack by

$$a = \frac{1}{\pi}\left(\frac{K_{Ic}}{\sigma_c}\right)^2. \quad (2)$$

The toughness of some samples was measured and yielded a value of $K_{Ic} \sim 2\ \mathrm{MPa}\sqrt{\mathrm{m}}$. This leads to a crack length $a \sim 0.5$ mm, which means that a crack of at least 0.5 mm within the sample would be needed for the failure due to crack propagation. As inspection of the samples never showed such long cracks, brittle failure is excluded (2) and (3). In Fig. 5b polymer pull-out and necking around nanoparticles is visible. Whether there is strong non-linear deformation of the polymer during pull-out is not clear. The visible network of PVB suggests that there is no PVB-film on the big grains left. Also the visible nanograins in Fig. 5d are detached from the polymer. It is not clear whether the detachment permanently exists or whether it is due to polymer pull-out. It is well known that PVB has a very good adhesion to ceramics in general, but the nano-grains seem to reduce the adhesion. Overall PVB seems to have a limited non-linear deformation which is strongly reduced in comparison to bulk PVB by the presence of alumina nano-grains. It might very well be that the grains prevent the

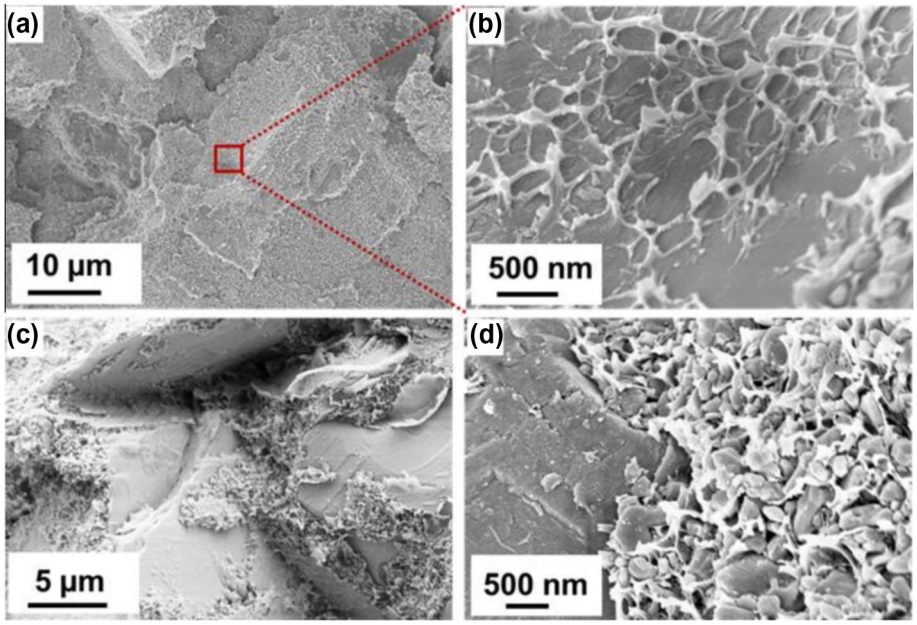

Fig. 5. (a) Fracture surface of a specimen after bending. (b) Magnification of (a) showing polymer pull out between nanograins. (c) Fracture surface of a controlled crack growth experiment. Areas without polymer pull out are visible. (d) Magnification of (c) showing detached nanoparticles from surrounding polymer.

plastic region from extending to a larger volume, such that plastic deformation occurs only in a small region within the sample (microplastic behavior), while the most part of it is deformed elastically. This is the mechanism leading to approx. 0.05–0.15 plastic strain.

4. Summary and conclusion

In conclusion, a novel processing concept was developed to generate large amounts of extremely highly filled ceramic polymer composites using spouted bed spray granulation and subsequent warm pressing. The material consists of up to 78 vol.% ceramic phase in a polymeric matrix, with a porosity of < 2 vol.%. This amount of hard and stiff constituents is still lower than in many biological materials, but has not been reached so far in appreciable amounts for artificial materials with an inherent isotropic and insulating structure. Four-point bending and tensile testing were carried out to determine the modulus of elasticity, the tensile strength, and the fracture strain as a function of the packing density. The measured modulus of elasticity was as high as 69 GPa. The fracture strain measured in tensile testing was on the order of 0.1%, which is much lower than the value for the unfilled polymer and in accordance with the generally observed phenomenon of massive loss of fracture strain for highly-filled composite materials. The measured tensile strength for the highest-filled samples was slightly above 50 MPa. Several failure mechanisms were discussed, which led to the conclusion that (1) failure due to crack propagation could be excluded, (2) failure due to limited poylmer–ceramic interfacial strength might play a role, but (3) that a failure mechanism based on local plastic deformation of the polymer (necking) is probably the major mechanism. Besides the mechanical properties, some major virtues which follow from the process route and the starting materials are that the material is, due to the filler type and the processing conditions, predominantly isotropic and can thus sustain two- and three-dimensional states of stress, it is biocompatible, insulating, and can easily be produced in large amount and also be disposed of as no potentially hazardous substances (such as fibers) are involved. By varying the processing parameters and starting materials, the mechanical properties can in principle be tailored within a very wide range, making it possible to adjust the mechanical behavior of the material. Furthermore, the fabrication method can easily be extended to polymers with higher yield points and tensile strengths. This opens up possible applications in many fields, including bone substitutes and artificial dentition. Further investigations will focus on achieving hierarchical materials design by prestructuring the ceramic particles, aiming at ultimately controlling and attune the force–displacement characteristics of man-made materials to match its respective demands in a way that nature has long since achieved.

Acknowledgements

We gratefully acknowledge financial support from the German Research Foundation (DFG) via SFB 986 "M^3", project A3 and A6, and from the Cluster of Excellence "Integrated Materials Systems" within the Landesexzellenzinitiative Hamburg, Germany.

References

[1] Jackson AP, Vincent JF, Turner RM. The mechanical design of nacre. Proc R Soc London Ser B 1988;234(1277):415–40.
[2] Barthelat F, Li C, Comi C, Espinosa HD. Mechanical properties of nacre constituents and their impact on mechanical performance. J Mater Res 2006;21(8):1977–86.
[3] Studart AR. Towards high-performance bioinspired composites. Adv Mater 2012;24:5024–44.
[4] Peterlik H, Roschger P, Klaushofer K, Fratzl P. From brittle to ductile fracture of bone. Nat Mater 2006;5(1):52–5.
[5] Imbeni V, Kruzic JJ, Marshall GW, Marshall SJ, Ritchie RO. The dentin–enamel junction and the fracture of human teeth. Nat Mater 2005;4(3):229–32.
[6] Bechtle S, Ang SF, Schneider GA. On the mechanical properties of hierarchically structured biological materials. Biomaterials 2010;31(25):6378–85.
[7] Gao H. Application of fracture mechanics concepts to hierarchical biomechanics of bone and bone-like materials. Int J Fract 2006;138(1–4):101–37.
[8] Fratzl P, Weinkamer R. Nature's hierarchical materials. Prog Mater Sci 2007;52(8):1263–334.
[9] Kim Y, Ribeiro L, Maillot F, Ward O, Eichhorn SJ, Meldrum FC. Bio-inspired synthesis and mechanical properties of calcite-polymer particle composites. Adv Mater 2010;22(18):20822086.
[10] Pouget E, Dujardin E, Cavalier A, Moreac A, Valery C, Marchi-Artzner V, et al. Hierarchical architectures by synergy between dynamical template self-assembly and biomineralization. Nat Mater 2007;6(6):434–9.
[11] Bonderer LJ, Studart AR, Gauckler LJ. Bioinspired design and assembly of platelet reinforced polymer films. Science 2008;319(5866):1069–73.
[12] Bonderer LJ, Studart AR, Woltersdorf J, Pippel E, Gauckler LJ. Strong and ductile platelet-reinforced polymer films inspired by nature: microstructure and mechanical properties. J Mater Res 2009;24(9):2741–54.
[13] Brandt K, Salikov V, Oezcoban H, Staron P, Schreyer A, Prado LASA, et al. Novel ceramic–polymer composites synthesized by compaction of polymer-encapsulated TiO(2)-nanoparticles. Compos Sci Technol 2011;72(1):65–71.
[14] Sellinger A, Weiss PM, Nguyen A, Lu YF, Assink RA, Gong WL, et al. Continuous self-assembly of organic–inorganic nanocomposite coatings that mimic nacre. Nature 1998;394(6690):256–60.
[15] Tang ZY, Kotov NA, Magonov S, Ozturk B. Nanostructured artificial nacre. Nat Mater 2003;2(6). p. 413-U8.
[16] Munch E, Launey ME, Alsem DH, Saiz E, Tomsia AP, Ritchie RO. Tough, bio-inspired hybrid materials. Science 2008;322(5907):1516–20.
[17] Arbatti M, Shan X, Cheng Z. Ceramic–polymer composites with high dielectric constant. Adv Mater 2007;19(10):13691372.
[18] Podsiadlo P, Kaushik AK, Arruda EM, Waas AM, Shim BS, Xu J, et al. Ultrastrong and stiff layered polymer nanocomposites. Science 2007;318(5847):80–3.
[19] Bonderer LJ, Feldman K, Gauckler LJ. Platelet-reinforced polymer matrix composites by combined gel-casting and hot-pressing. Part I: polypropylene matrix composites. Compos Sci Technol 2010;70(13, SI):1958–65.
[20] Wardle BL, Saito DS, Garcia EJ, Hart AJ, de Villoria RG, Verploegen EA. Fabrication and characterization of ultrahigh-volume-fraction aligned carbon nanotube-polymer composites. Adv Mater 2008;20(14). 2707+.
[21] German RM. Particle packing characteristics. Princeton (NJ): Metal Powder Industries Federation; 1989.
[22] McGeary RK. Mechanical packing of spherical particles. J Am Ceram Soc 1961;44(10):513–22.
[23] Mathur KK, Epstein N. Spouted beds. New York: Academic Press; 1974.
[24] Epstein N, Grace JR, editors. Spouted and spout-fluid beds: fundamentals and applications. Cambridge: Cambridge University Press; 2011.
[25] Fries L, Antonyuk S, Heinrich S, Palzer S. DEM-CFD modeling of a fluidized bed spray granulator. Chem Eng Sci 2011;66(11):2340–55.
[26] Teunou E, Poncelet D. Batch and continuous fluid bed coating – review and state of the art. J Food Eng 2002;53(4):325–40.
[27] Vuthaluru HB, Zhang DK. Effect of coal blending on particle agglomeration and defluidisation during spouted-bed combustion of low-rank coals. Fuel Process Technol 2001;70(1):41–51.
[28] Lukasiewicz SJ. Spray-drying ceramic powders. J Am Ceram Soc 1989;72(4):617–24.
[29] Olazar M, Sanjose MJ, Aguayo AT, Arandes JM, Bilbao J. Stable operation conditions for gas solid contact regimes in conical spouted beds. Ind Eng Chem Res 1992;31(7):1784–92.
[30] Parks GA. Isoelectric points of solid oxides, solid hydroxides, and aqueous hydroxo complex systems. Chem Rev 1965;65(2). p. 177-&.
[31] Litster J, Ennis B. The science and engineering of granulation processes. Dordrecht (The Netherlands): Kluwer Academic Publishers; 2004.
[32] Link JM, Godlieb W, Deen NG, Kuipers JAM. Discrete element study of granulation in a spout-fluidized bed. Chem Eng Sci 2007;62(1–2):195–207.
[33] Antonyuk S, Heinrich S, Smirnova I. Discrete element study of aerogel particle dynamics in a spouted bed apparatus. Chem Eng Technol 2012;35(8, SI):1427–34.
[34] Geldart D. Types of gas fluidization. Powder Technol 1973;7(5):285–92.
[35] van Ommen JR, Nijenhuis J, Coppens M. Reshaping the structure of fluidized beds. Chem Eng Prog 2009;105(7):49–57.
[36] Markowski A, Kaminski W. Hydrodynamic characteristics of jet-spouted beds. Can J Chem Eng 1983;61(3):377–81.
[37] Jelitto H, Felten F, Swain MV, Balke H, Schneider GA. Measurement of the total energy release rate for cracks in PZT under combined mechanical and electrical loading. J Appl Mech 2007;74(6):1197.
[38] Gere MG. Mechanics of materials. 6th ed. Belmont CA (USA): Bill Stenquist; 2004.
[39] Wang M, Joseph R, Bonfield W. Hydroxyapatite–polyethylene composites for bone substitution: effects of ceramic particle size and morphology. Biomaterials 1998;19(24):2357–66.
[40] Cahn R, Haasen P, Kramer E, Mughrabi H, editors. Materials science and technology: plastic deformation and fracture of materials. A comprehensive treatment. New York (Weinheim): VCH Publishers Inc.; 1993.